Eur Food Res Technol (2015) 241:553–572
DOI 10.1007/s00217-015-2484-0

ORIGINAL PAPER

A theoretical study of the antioxidant properties of phenolic acid amides investigated through the radical-scavenging and metal chelation mechanisms

Mwadham M. Kabanda[1,2]

Received: 9 April 2015 / Revised: 2 June 2015 / Accepted: 6 June 2015 / Published online: 20 June 2015

Abstract Phenolic amides have been investigated extensively as efficient antioxidant compounds by means of experimental techniques. However, their mode of action has not been determined through the use of theoretical approaches. In this study, theoretical studies on the conformational and antioxidant properties of phenolic acid amides were performed to investigate factors that contribute to their conformational preferences and to elucidate their antioxidant properties and mechanisms. The antioxidant activity of selected phenolic acid amides has been considered through the ability of the compounds to scavenge free radical species and chelate metal ions. The antiradical mechanisms were investigated using the B3LYP/6-311+G(d,p) method, and the metal chelation mechanism was investigated using the B3LYP/6-311+G(3df,2p)//B3LYP/6-311+G(d,p) method. The results show that the preferred conformers for the neutral and anionic conformers are stabilised by the presence of intramolecular hydrogen bonds (IHBs). The neutral and cationic radical species are stabilised by both IHBs and the spin density delocalisation of the unpaired electron. The preferred Cu complex is one in which the Cu ion interacts simultaneously with the carbonyl group and the benzene ring of the aromatic amine moiety. An estimated metal ion affinity is influenced by the nature of the ligand and the media. In comparison with the isolated Cu(II) ion, the charge on the coordinated metal ion decreases from 2 to ~1 suggesting that the Cu ion is reduced on interaction with the ligand molecule undergoes oxidation.

Keywords Phenolic acid amides · Metal chelation mechanism · Electron transfer mechanism · Intramolecular hydrogen bonding · AIM bonding analysis

Abbreviations

MIA	Metal ion affinity
IHB	Intramolecular hydrogen bond
ROS	Reactive oxygen species
RNS	Reactive nitrogen species
DFT	Density functional theory
HAT	Hydrogen atom transfer
SET	Single-electron transfer
SET-PT	Single-electron transfer followed by proton transfer
SPLET	Sequential proton loss electron transfer
BDE	Bond dissociation enthalpy
AIP	Adiabatic ionisation potential
PDE	Proton dissociation enthalpy
ETE	Electron transfer enthalpy
PA	Proton affinity
TMC	Transition metals chelation
NBO	Natural bond order
AIM	Atoms in molecule
CP	Critical point
BCP	Bond critical point

Electronic supplementary material The online version of this article (doi:10.1007/s00217-015-2484-0) contains supplementary material, which is available to authorized users.

✉ Mwadham M. Kabanda
mwadham.kabanda@nwu.ac.za

[1] Department of Chemistry, Faculty of Agriculture, Science and Technology, School of Mathematical and Physical Science, North-West University (Mafikeng Campus), Private Bag X2046, Mmabatho 2735, South Africa

[2] Material Science Innovation and Modelling (MaSIM) Research Focus Area, Faculty of Agriculture, Science and Technology, North-West University (Mafikeng Campus), Private Bag X2046, Mmabatho 2735, South Africa

Introduction

Many biochemical reactions in our body involve the generation of reactive oxygen species (ROS) or reactive nitrogen species (RNS). Under normal conditions, the balance between the generation and reduction in ROS is controlled by the body's antioxidant defence mechanism. However, under certain pathological conditions, when ROS are not effectively eliminated by the body's antioxidant defence mechanism, the dynamic balance between the generation and elimination of ROS is broken. As a result, ROS may attack the biomolecules such as lipids, carbohydrates, proteins and DNA, causing cellular damage and resulting in oxidative stress. The consequence of cellular damage is the development of various degenerative diseases such as cardiovascular, neurodegenerative and Alzheimer's diseases, and cancers [1–4]. In order to protect against cellular damage by ROS, both synthetic and natural antioxidant molecules are increasingly utilised to enhance the antioxidant capability of the body system. However, synthetic antioxidants are less preferred to natural products because of their adverse side effects on some of the body organs, such as liver [5–7]. Thus, considerable attention has been given to the search for natural antioxidants (often from plant sources). The current study focuses on the antioxidant potential of phenolic acid amide derivatives. These compounds have been reported both as natural products and as synthetic products. They possess various biological activities including antibacterial, antiviral, anti-inflammatory, antioxidative, and antiproliferative [8–14]. Phenolic acid amides are conjugates of aromatic amines to phenolic acids. Both aromatic amines and phenolic acids have been reported to possess antioxidant activities [15–20]. Therefore, a study of the antioxidant activity of phenolic acid amides would yield useful information on the effect of conjugation of the constituent molecules on the antioxidant properties of the phenolic acid amides. The aromatic amines selected for the study are phenylethylamine, tyramine and dopamine, and the phenolic acids selected for the study are cinnamic acid, coumaric acid and caffeic acid. The conjugated phenolic acid amides selected for the study include caffeoyltyramine (CaTy), caffeoyldopamine (CaD), caffeoylphenylethylamine (CaPEA), cinnamoyldopamine (CiD) and *p*-coumaroyldopamine (*p*-CoD). The structures of the selected compounds are shown in Fig. 1 together with the atom numbering interesting for the discussion of the study.

Although extensive experimental and theoretical studies on the antioxidant activity of the isolated aromatic amines and phenolic acids have been reported [20–26], only experimental findings have been reported extensively on the antioxidant activity of phenolic acid amide derivatives [10, 12, 14, 27]. Therefore, the objective of this work is to study the electronic and molecular properties of these compounds in order to understand the mechanism of their antioxidant activity and to compare the information thereof with that of the constituent phenolic acids and aromatic amines. The study is performed utilising the density functional theory (DFT) with the B3LYP functional, for both the study of both the antiradical activity and the metal chelation mechanism. The calculations are performed *in vacuo*, in benzene, in acetonitrile and in water solvents. The investigation in different media is meant to mimic the different aqueous and

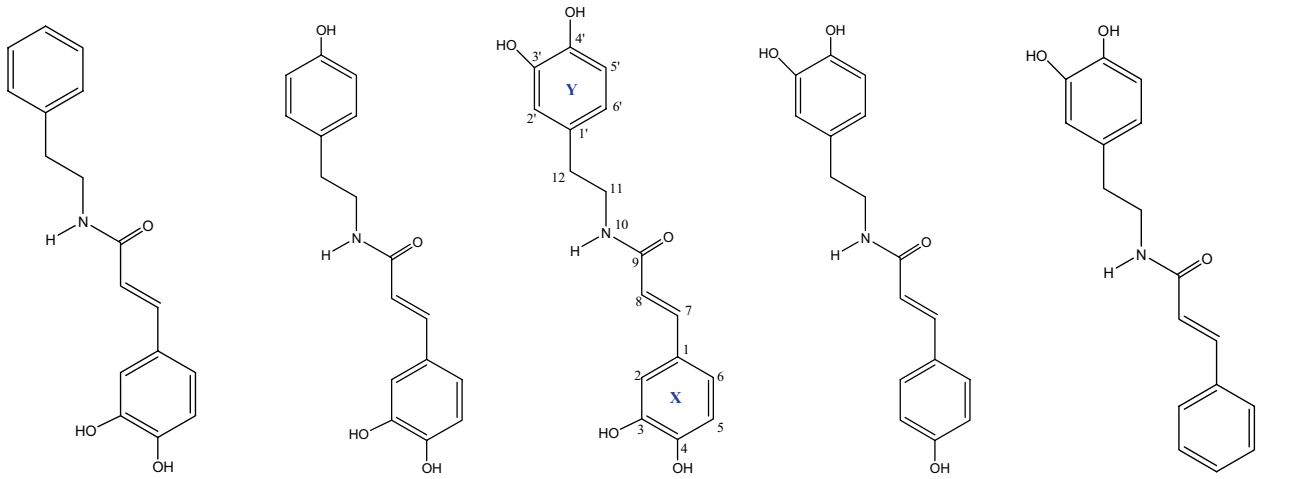

Fig. 1 Schematic representation of the studied phenolic acid amides, and the atom numbering for the main skeletal is shown on caffeonyldopamine structure. The O atoms and the H atoms are given the number of the C atom to which they are bonded. The phenolic acid ring is denoted X and the aromatic amine ring is denoted Y

lipophilic environments found in biological systems where antioxidants interact with both radical species and toxic transition metal ions [4, 28, 29].

The schematic representation of the selected phenolic acid amide derivatives and the atom numbering utilised in this work are shown in Fig. 1. The structures are arranged in order of increasing number of hydroxyl groups on the aromatic amine ring (ring Y) and decreasing number of hydroxyl groups on the phenolic acid ring (ring X). The two main torsional degrees of freedom about the aliphatic chain (the C1′–C12–C11–N10 and the C12–C11–N10–C9′ torsion angles) and the single C−O bonds, connecting the OH groups to the aromatic rings, are flexible, and their rotation may result in several possible conformations. Because of the presence of catecholic moiety (moieties) in all the compounds, it is expected that all the compounds can be stabilised by intramolecular hydrogen bonds (IHB) involving the phenolic OH groups at C3 and C4 or those at C3′ and C4′. IHB are known to play significant roles in stabilising molecular conformations and in influencing biological activities [30–42]. For instance, the antioxidant activities of several biological molecules have been reported to be enhanced by the presence of the IHB because of the role of this interaction is stabilising the radical species formed due to the transfer of the hydrogen atom or the electron [3, 4, 29, 43, 44].

The assessment of antioxidant properties by a single mechanism underestimates the antioxidant potential for that particular molecule because it reflects only the ability to inhibit a precise class of oxidants present. To this effect, the current study investigates the antioxidant mechanism of phenolic acid amides through both the antiradical and the metal chelation mechanisms. The antiradical-scavenging activity is often discussed through four mechanisms, the hydrogen atom transfer (HAT, [45–47]), the single-electron transfer (SET, [48]), the single-electron transfer followed by proton transfer (SET-PT, [49]) and the sequential proton loss electron transfer (SPLET, [50]) mechanisms. The HAT, SET-PT and SPLET mechanisms depend on the presence of free phenolic OH group(s). The HAT mechanism is related to the ability of the molecule to donate its phenolic H atom to the radical species:

$$R^{\cdot} + ArOH \rightarrow RH + ArO^{\cdot} \quad (1)$$

The termination of further chain reactions depends on the stability of the neutral radical intermediates ($ArO^{\cdot}$ radical species) formed. This means that factors enhancing the stability of the $ArO^{\cdot}$ radical species, such as the resonance delocalisation of the electron within the aromatic ring and the formation of the quinine structure, increase the antiradical activity. The ability of phenolic antioxidants to donate a hydrogen atom is mainly governed by the homolytic O–H bond dissociation enthalpy (BDE).

The SET mechanism is governed by the capacity of an antioxidant compound to transfer an electron and reduce any other compound including metal ions and radical species. In the case of antioxidant reactions involving radical species, the antioxidant compound (ArOH) transfers a single electron to the radical species ($R^{\cdot}$):

$$R^{\cdot} + ArOH \rightarrow ArOH^{\cdot+} + R^{-} \quad (2)$$

Relative reactivity in SET mechanism is primarily determined by adiabatic ionisation potential (AIP) value [51, 52] of the reactive functional group. The lower the AIP value, the more favourable the electron transfer reaction [48, 53].

The single-electron transfer followed by proton transfer (SET-PT, [49]) is a two-step reaction mechanism. In the first step, a phenolic antioxidant molecule reacts with the free radical giving rise to the cationic radical form of the phenolic antioxidant and an anionic form of the radical.

$$R^{\cdot} + ArOH \rightarrow ArOH^{\cdot+} + R^{-} \quad (3.1)$$

This reaction is a thermodynamically significant step of this two-step mechanism. In the second step, the cationic radical form of the phenolic antioxidant decomposes into a phenolic radical and a proton.

$$ArOH^{\cdot+} \rightarrow ArO^{\cdot} + H^{+} \quad (3.2)$$

The numerical parameters related with the SET-PT mechanism are the adiabatic ionisation potential (AIP) for the first step and proton dissociation enthalpy (PDE) for the second step.

The sequential proton loss electron transfer reaction is also a two-step reaction mechanism. In the first step, the phenolic antioxidant dissociates into an anionic form and proton,

$$ArOH \rightarrow ArO^{-} + H^{+} \quad (4.1)$$

In the second step, the ions created in the first reaction react with the free radical giving rise to the radical form of the phenolic antioxidant as well as a neutral molecule.

$$ArO^{-} + X^{\cdot} + H^{+} \rightarrow ArO^{\cdot} + XH$$

The numerical parameters related with this mechanism are the proton affinity (PA), for the first reaction step, and electron transfer enthalpy (ETE) for the second step.

The other mechanism used to describe antioxidant properties is transition metals chelation (TMC, [45]). Transition metals have the ability to catalyse oxidative processes leading to the formation of hydroxyl radical species and

$$ArOH \rightarrow ArO^{-} + H^{+} \quad (5.1)$$

Transition metals also have the ability to decompose hydroperoxides through the Fenton reaction:

$$H_2O_2 + M^{n+} \rightarrow HO^{-} + HO^{\cdot} + M^{(n+1)+} \quad (5.2)$$

In the TMC mechanism associated with the formation of the hydroxyl radical species (Eq. 5.1), each molecule which may dissociate has the ability to chelate transition metal ions. In particular, anions of polyphenols have the significant abilities to chelate transition metal ions. Since chelation of metals often occurs due to deprotonated hydroxyls in the polyphenols, the ability of a molecule to produce the proton is taken into consideration. The numerical parameter related with this mechanism is the gas-phase acidity, which is identified with the vacuum enthalpy of the compound ($\Delta H_{\text{acidity}}$). For the calculations in solvent media, the free Gibbs energy ($\Delta G_{\text{acidity}}$) is the parameter of interest.

Although the metal chelation mechanism is considered a minor reaction in comparison with radical-scavenging mechanisms [54], its occurrence in biological systems plays significant role in the removal of toxic transition metal ions through altering their redox potentials thereby rendering them inactive. In cases where the metal chelation mechanism is possible, it is governed by the ability of the antioxidant molecule to reduce the transition metal ion (by donating electrons to the metal ion) and to form a stable metal–ligand complex. The formation of a stable complex structure, as a result of the interaction of the antioxidant (ligand) with the toxic transition metal ion, shields biological targets from the metal ion (e.g. Fe^{2+}, Fe^{3+}, Cu^{2+}, …), thereby preventing metal-catalysed free radical reactions [54, 55].

Phenolic acid amide derivatives, with their multiple hydroxyl groups, aromatic rings and the carbonyl group on the aliphatic chain, have several available sites for metal complexation. However, there has not been any investigation concerned with the formation of stable complexes between phenolic acid amides and transition metals ions. This study considers the possible 1:1 stoichiometry that metal/phenolic acid amide complexes can exhibit. The copper(II) cation (Cu^{2+}) has been selected for the investigation mainly because Cu and Fe are the most abundant transition metal ions in biological systems.

Computational details

The geometry optimisations for the neutral species and the radical species of phenolic acid amides were performed with the DFT/B3LYP method using the 6-311+G(d,p) basis sets [28, 56–58]. The restricted wave function was employed for the closed-shell neutral species, and the unrestricted wavefunction was utilised for the open-shell radical species. Geometry optimisation of each $ArO^{\cdot}$ radical was performed starting from the optimised structure of the parent molecule, after the H atom was removed from the possible position. Frequency calculations were performed, at the same level of calculations as the geometry optimisation, on fully optimised conformers, to determine the nature of the stationary points. Zero-point and thermal enthalpies corrections, computed at $T = 298$ K and $p = 1$ atm in the rigid rotor harmonic oscillator approximation, were performed to obtain free energies and enthalpies. Solvent effects on geometries and relative conformational stabilities have been taken into consideration using the solvent model density (SMD) model [59]. Calculations in different media were performed using the B3LYP/6-311+G(d,p) method and starting from the optimised geometries *in vacuo*. The utilisation of the geometry obtained *in vacuo* for calculations in the presence of the solvent allows for the possibility of tracking geometry changes as a result of the geometry relaxation in solution.

The adiabatic ionisation potential (AIP) was estimated using the equation [48, 53]

$$\text{AIP} = \text{H}\left(\text{M}^{\cdot+}\right) - \text{H}(\text{M}) \tag{6}$$

where M is the lowest-energy conformer for each of the studied compounds, $H(M^{\cdot+})$ is the enthalpy of the M cation radical species, and H(M) is the enthalpy of M. The bond dissociation enthalpy (BDE) was estimated by using the equation

$$\text{BDE} = \text{H}_\text{r}\left(\text{ArO}^{\cdot}\right) + \text{H}_\text{h}\left(\text{H}^{\cdot}\right) - \text{H}_\text{p}(\text{ArOH}) \tag{7}$$

where H_r is the enthalpy of the radical generated by H abstraction, H_h is the enthalpy of the H atom, and H_p is the enthalpy of parent compound. A low O–H BDE value, usually associated with greater ability to donate the H atom, corresponds to high radical-scavenging ability by the phenolic compound [45, 46]. Proton dissociation enthalpy (PDE) has been calculated using the equation

$$\text{PDE} = \text{H}^{\cdot}_{\text{ArO}} + \text{H}^{+}_{\text{H}} - \text{H}^{\cdot+}_{\text{ArOH}} \tag{8}$$

in which $H^{\cdot}_{ArO}$ is the enthalpy of the radical, H^{+}_{H} is the enthalpy of the proton, $H^{\cdot+}_{ArOH}$ is the enthalpy of cationic radical. Proton affinity has been estimated by using the equation

$$\text{PA} = \text{H}^{-}_{\text{ArO}} + \text{H}^{+}_{\text{H}} - \text{H}_{\text{ArOH}} \tag{9}$$

where, H^{-}_{ArO} is the enthalpy of the anion, H^{+}_{H} is the enthalpy of the proton, H_{ArOH} is the enthalpy of the compound. Electron transfer enthalpy (ETE) has been estimated using the equation

$$\text{ETE} = \text{H}^{\cdot}_{\text{ArO}} - \text{H}^{-}_{\text{ArO}} \tag{10}$$

where $H^{\cdot}_{ArO}$ is the enthalpy of the radical and H^{-}_{ArO} is the enthalpy of the anion.

The $CaD\cdots Cu^{2+}$ complexes were optimised using UB3LYP/6-311+G(d,p) method. Harmonic vibrational frequencies were obtained at the same level of theory to classify the stationary points as local minima or transition states. For all the local minima, final energies were

obtained, on the aforementioned UB3LYP/6-311+G(d,p) optimised geometries, by using a 6-311+G(3df,2p) basis set that includes diffuse functions on all heavy atoms, as well as high angular momentum functions, which may be important when describing π-complexes. For Cu the 6-311+G(3df,2p) basis set corresponds actually to the (14s9p5d/9s5p3d) Wachters–Hay [60–63] basis supplemented with a set of (1s2p1d) diffuse functions and with two sets of f functions (rather than d) and one set of g functions (rather than f).

The CaD···Cu^{2+}-binding energy was estimated using the following equation:

$$\Delta E_{\text{binding}} = -\Delta E_{\text{inter}} = \left(E^{2+}_{\text{CaD}\cdots\text{Cu}} - E^{2+}_{\text{Cu}} - E_{\text{CaD}}\right) \quad (11)$$

where ΔE_{inter} is the interaction energy, $E^{2+}_{\text{CaD}\cdots\text{Cu}}$ is the total energy of the optimised complex, E^{2+}_{Cu} is the total energy of the isolated Cu^{2+} cation, and E_{CaD} is the total energy of the isolated CaD conformer. The greater the computed value of the binding energy, the stronger the affinity of M^{2+} ion to bind to the ligand [64, 65].

All calculations were performed with Gaussian09 programme [66]. The schematic representations were drawn using the ChemOffice package in the UltraChem 2010 version, and conformers were drawn using GaussView5 programme.

The natural bond order (NBO) and the atoms-in-molecule (AIM) population analysis schemes were utilised for gaining insight into the bonding situation of the metal···molecule complexes. NPA charges on the atoms were determined by means of the natural bond order (NBO) analysis scheme [67–69]. The atoms-in-molecule (AIM) procedure was performed using the AIMAll programme [70]. The number of critical points (CP) found for the metal–ligand systems are in agreement with the Poincare–Hopf rule. The following parameters of the bond critical point (BCP) were analysed: the electron density (ρ) and its Laplacian ($\nabla^2\rho$), the density of the total energy of electrons (H), and its two components, the Lagrangian kinetic electron density (G) and the potential electron density (V). The total energy density, H, was estimated as the sum of the kinetic electron density (G) and potential energy density (V):

$$H_{\text{BCP}} = G_{\text{BCP}} + V_{\text{BCP}} \quad (12)$$

Results and discussion

Geometrical and conformational stabilities for the isolated molecules

The optimised conformers of the neutral studied compounds are shown in Fig. 2, and their relative energies are reported in Table 1. The conformers shown are those differing in terms of the rotation about the OH groups. In all the structure, the lowest-energy conformers are stabilised by the IHB formed in the catecholic unit. The $–CH_2CH_2NH–$ group prefers a near-perpendicular orientation with respect to ring Y, while the –CH=CHC(O)– prefers a planar arrangement with respect to ring X. *In vacuo*, the relative energy difference among conformers of each structure is so small (often <1 kcal/mol) that all conformers can be considered to exits. A study in different media shows that the energy difference between conformers is always below 1 kcal/mol and that as the solvent polarity increases, the energy order may be reversed. This result suggests that all the conformers (for each structure) can be considered populated and should be taken into consideration on further studies of the activities of the compound. However, because conformational differences have minimal effect on the antioxidant activity properties (such as BDE values [58, 71]), only the lowest-energy conformers have been taken into consideration for the study of the antiradical activity of phenolic acid amide derivatives.

Antioxidant properties and the hydrogen atom transfer (HAT) mechanism

The optimised neutral radical species for each of the studied phenolic amide derivative are shown in Fig. 3, the corresponding molecular spin density distributions are shown in Fig. S1, and their relative energies are reported in Table 1. The radical species are named by including the notation "rad" in the name, and the number of the O atom on which the H atom is abstracted. Only the H atom that is not engaged in IHB has been abstracted because of the knowledge that IHB is important in influencing antioxidant activity [29]. The optimised radical species are stabilised by the presence of IHB, either involving the radicalised O atom as the H atom acceptor or present in the ring on which there has not been H atom abstraction. In all the structures with catecholic unit, the lowest-energy radical species correspond to the abstraction of the H atom from the *para* position. When the H atom is abstracted from the phenolic acid ring, the energy difference between the *para* and the *meta* radical species is nearly 3 kcal/mol, while when the H atom is abstracted from the aromatic amine ring, the energy difference between the *para* and the *meta* radical species is lower, being <1 kcal/mol.

The ability of the molecule to donate its hydroxyl H atom is better assessed by estimating the bond dissociation enthalpy for that O–H group. A lower BDE value means that there is high tendency for the molecule to donate its H atom, which in turn implies high reactivity and therefore high antiradical activity. Usually one compares the BDE value for the removal of any of the OH group in a given

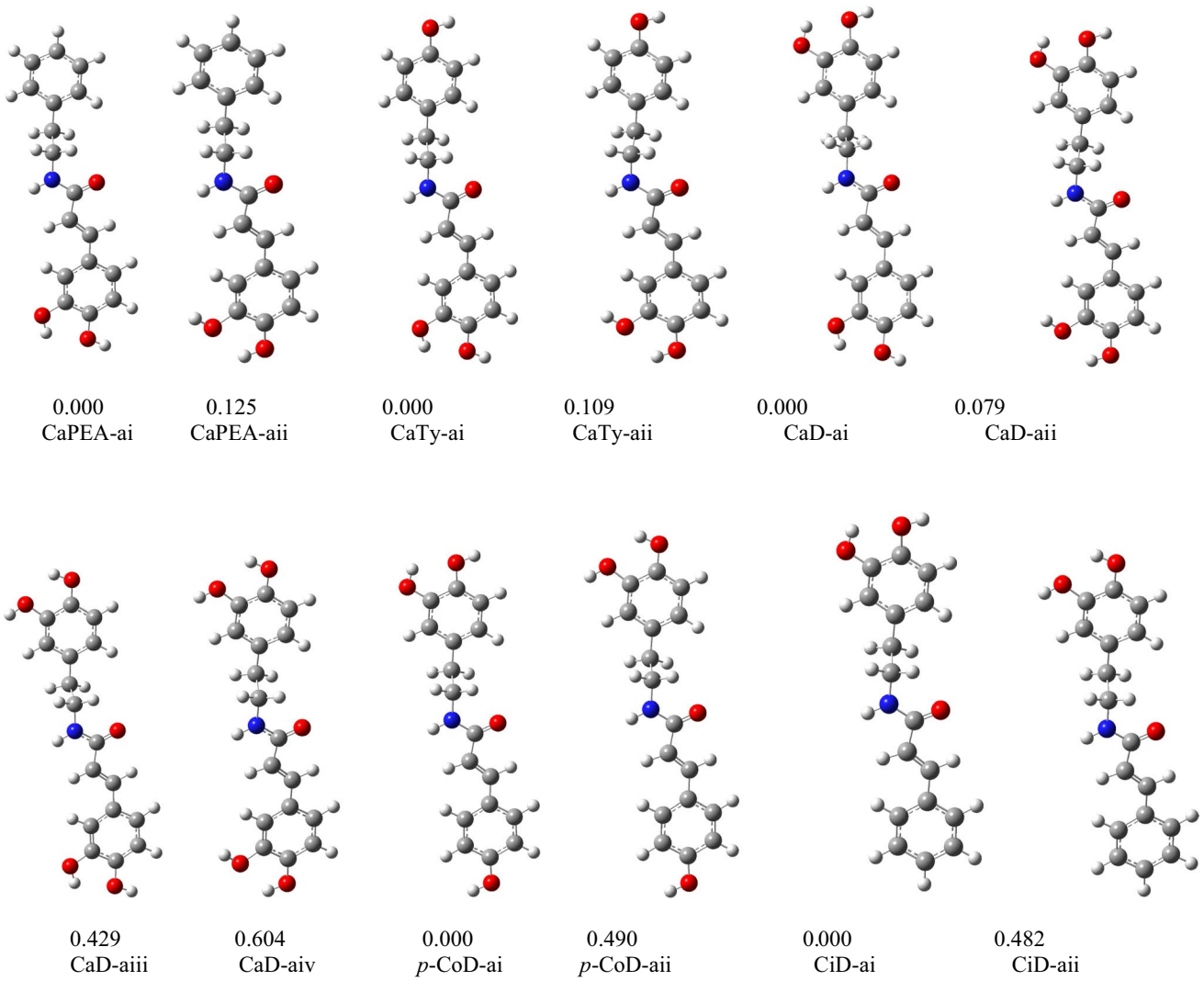

Fig. 2 Optimised lowest-energy conformers of the studied phenolic acid amides, B3LYP/6-311+G(d,p) results *in vacuo*. For a given structure, relative energy values are shown below each conformer. The results in solution are similar to the results *in vacuo*

molecule with the BDE value for a removal of the H atom from some standard antioxidant molecules or molecules that are already known as good antioxidant. The BDE values for the studied phenolic acid amides are reported in Table 2. An abstraction of the H atom in *para* position results in lower BDE value than an abstraction of the H atom in *meta* position. The BDE value for the phenolic units (CaTy-aii-A, CaTy-ai-A, *p*-CoD-aii-C and *p*-CoD-ai-A) is higher (79–81 kcal/mol) than the O–H BDE values for the catecholic units (72–75 kcal/mol). The estimated BDE values, for the different radical species, are within the range of most substituted catechol and phenol derivatives. For instance, the estimated values of the BDE values of phenolic acid amides are close to those of rooperol and quercetin [29, 72].

A comparison of the BDE value obtained from catecholic units suggests that it is slightly lower for the case in which the catechol moiety is on the phenolic acid ring (CaPEA-ai-C and CaTy-ai-C) than for the aromatic amine ring (*p*-CoD-ai-A and CiD-ai-A). A similar comparison of the BDE values obtained from the phenolic unit of the aromatic amine ring and that of the phenolic acid ring shows a similar trend.

For each of the studied compound, the BDE values increase with the increase in solvent polarity, which implies that the phenolic acid amides are better H atom abstractor in non-polar media than in polar media. In polar media, an intermolecular H-bond can form between the phenolic hydroxyl, especially a catechol group, and the solvent molecule. The formation of such molecule···solvent intermolecular H-bonds may hamper the H atom-donating ability [73, 74], resulting in high BDE values in polar solvents.

Analysis of the spin density distribution (Fig. S1) suggests that the distribution of the single electron is

Table 1 Relative energy (kcal/mol) for the conformers of neutral species, neutral radical species and anionic species of the studied phenolic acid amides, B3LYP/6-311+G(d,p) results in different media

Structure	*In vacuo*	In benzene	In acetonitrile	In water
Neutral conformers				
CaPEA-ai	0.000	0.000	0.000	0.016
CaPEA-aii	0.125	0.169	0.004	0.000
CaTy-ai	0.000	0.000	0.000	0.026
CaTy-aii	0.109	0.154	0.000	0.000
CaD-ai	0.000	0.000	0.014	0.000
CaD-aii	0.079	0.130	0.000	0.023
CaD-aiii	0.429	0.401	0.061	0.041
CaD-aiv	0.604	0.596	0.074	0.054
p-CoD-ai	0.000	0.000	0.000	0.000
p-CoD-aii	0.490	0.449	0.039	0.007
CiD-ai	0.000	0.000	0.000	0.000
CiD-aii	0.482	0.441	0.040	0.0023
Neutral radical conformers				
CaPEA-ai-rad-O4	0.000	0.000	0.000	0.000
CaPEA-aii-rad-O3	3.045	3.143	3.120	2.974
CaTy-ai-rad-O4	0.000	0.000	0.000	0.000
CaTy-aii-rad-O3	3.060	3.140	2.974	2.887
CaTy-ai-rad-O4′	9.280	8.546	7.090	6.057
CaTy-aii-rad-O4′	9.447	8.739	7.151	6.150
CaD-ai-rad-O4	0.000	0.000	0.000	0.377
CaD-ai-rad-O4′	0.756	0.642	0.222	0.000
CaD-aiii-rad-O3′	1.348	1.323	1.087	0.970
CaD-aii-rad-O3	3.082	3.111	3.078	3.272
p-CoD-ai-rad-O4′	0.000	0.000	0.000	0.000
p-CoD-aii-rad-O3′	0.568	0.704	0.904	0.929
p-CoD-aii-rad-O4	7.614	6.990	6.085	5.718
p-CoD-ai-rad-O4	7.110	6.544	5.991	5.655
CiD-ai-rad-O4′	0.000	0.000	0.000	0.000
CiD-aii-rad-O3′	0.557	0.686	1.467	0.829
Anionic conformer				
CaPEA-ai-an-O4	0.000	0.000	0.000	0.000
CaPEA-aii-an-O3	4.796	3.731	2.668	2.110
CaTy-ai-an-O4	0.000	0.000	0.000	0.000
CaTy-aii-an-O3	4.789	3.732	2.663	2.118
CaTy-aii-an-O4′	21.780	16.930	10.97	7.754
CaTy-ai-an-O4′	22.640	17.350	11.11	7.955
CaD-ai-an-O4	0.000	0.000	0.000	0.000
CaD-aii-an-O3	4.795	3.714	2.663	2.127
CaD-ai-an-O4′	12.500	9.564	5.670	4.353
CaD-aiii-an-O3′	12.810	9.100	5.178	4.042
p-CoD-aii-an-O4	0.000	0.073	0.084	0.025
p-CoD-ai-an-O4′	0.114	0.000	0.041	0.000
p-CoD-aii-an-O3′	4.450	2.021	0.000	0.511
p-CoD-ai-an-O4	4.726	2.474	0.326	0.584
CiD-ai-an-O4′	0.000	0.000	0.000	0.000
CiD-aii-an-O3′	0.000	0.637	0.090	0.331

determined by the site on the ring at which the H atom is abstracted. When the H atom is abstracted from a *para* position, the distribution of the single electron is delocalised furthest from the radicalised O atom than when the H atom is abstracted from the *meta* position. In the former case, the single electron may be distributed to a large extent up to the C=O and N–H groups of the aliphatic chain, while in the latter cases, the spin density distribution is largely on the *ortho* and *para* positions with respect to the radicalised O3 atom. An analysis of the atomic spin density of the radicalised O atom (Table 1) suggests that radical species with the least atomic spin density on the radicalised O atom have the lowest BDE value. Consistently, the more delocalised the spin density in the radical is, the easier is the radical formed and thus the lower is the BDE. The stability of the radical species of phenolic acid amides is therefore influenced to a large extent by the delocalisation of the spin density of the single electron, from the atom on which the H atom is abstracted [29]. Therefore, both IHB and spin delocalisation play significant role in the stabilisation of the neutral radical species formed from H atom transfer.

An investigation on the N–H bond dissociation enthalpy of the central N–H group was performed in order to be compared with the O–H BDE results. The outcome is reported in Table S2 and indicates that the H atom abstraction from the N–H group is very difficult because the N–H BDE value (~102 kcal/mol) is much higher than that of O–H BDE. A comparison across structures suggests that the N–H BDE value is constant across structures. The calculated spin density of O atom in phenoxyl radical derived from a given molecule is lower than that of N in N-centred radical derived from the same molecule. The two factors suggest that the hydrogen atom transfer antioxidant mechanism of phenolic acid amides is a result of H atom abstraction from the phenolic OH group rather than from the N–H group.

A comparison of the BDE values of the isolated aromatic amines (tyramine and dopamine) and phenolic acids (caffeonic acid and coumaric acid, Table S1) suggests that aromatic amines are better H atom donor than phenolic acids. A comparison of the BDE values of the isolated aromatic amines and phenolic acids with the BDE for the phenolic acid amides suggests that the conjugation of the two units results in lower BDE value.

The single-electron transfer (SET) mechanism

The calculated ionisation potential (IP) values, which characterise the electron transfer mechanism, are reported in Table 1 for all the compounds. *In vacuo*, the order of the IP values is such that CaD < *p*-CoD < CaTy < CiD < CaPEA. The IP values therefore depend on the number and the

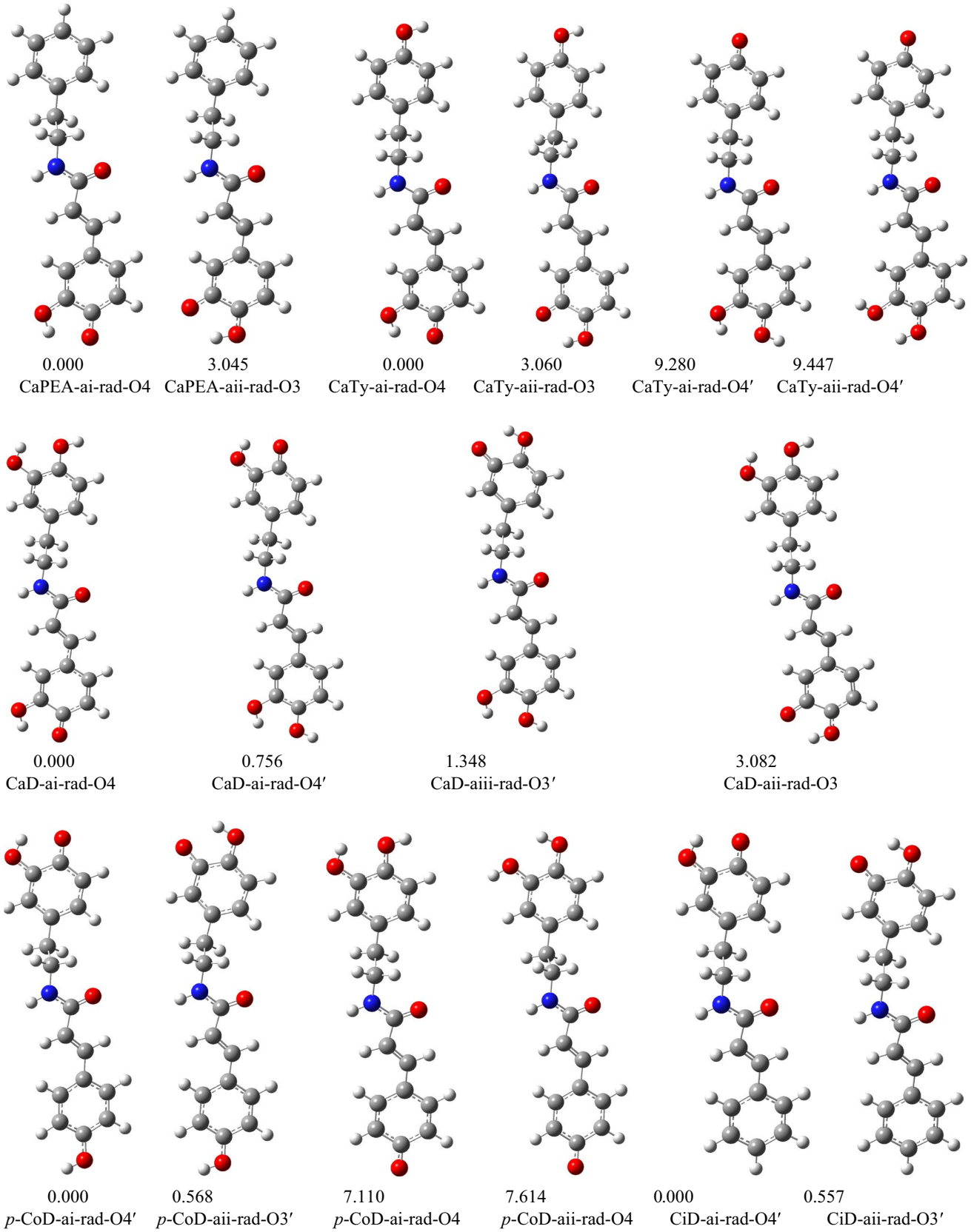

Fig. 3 Optimised lowest-energy conformers of the studied phenolic acid amides neutral radical species, B3LYP/6-311+G(d,p) results *in vacuo*. For a given structure, relative energy values are shown below each conformer. The results in solution are similar to the results *in vacuo*

Table 2 Antioxidant descriptors for all the studied compounds, B3LYP/6-311+G(d,p) results in different media

Structure	Media	BDE (kcal/mol)	IP (kcal/mol)	PDE (kcal/mol)	PA (kcal/mol)	ETE (kcal/mol)	Spin density on the radicalised O
CaPEA-ai-O4	In vacuo	72.032	171.034	219.150	326.450	63.649	0.2890
	In benzene	72.180	149.371	28.092	93.907	83.433	0.2822
	In acetonitrile	73.564	129.896	13.741	43.175	100.417	0.2738
	In water	75.901	128.774	1.853	23.856	106.74	0.2632
CaPEA-aii-O3	In vacuo	74.992		216.104	321.739	65.400	0.3386
	In benzene	75.200		24.949	90.299	84.021	0.3298
	In acetonitrile	76.640		10.621	40.552	99.965	0.3190
	In water	78.844		−1.121	21.777	105.876	0.3027
CaTy-aii-O4′	In vacuo	81.377	166.156	230.400	343.483	53.001	0.4020
	In benzene	80.799	146.476	36.565	107.158	75.781	0.3866
	In acetonitrile	80.667	129.807	17.863	51.489	96.131	0.3644
	In water	81.974	128.696	5.206	29.417	104.309	0.3386
CaTy-aii-O3′	In vacuo	74.990		224.013	326.487	63.610	0.3385
	In benzene	75.200		30.966	93.956	83.385	0.3297
	In acetonitrile	76.490		13.686	43.178	100.264	0.3189
	In water	78.712		1.943	23.781	106.682	0.3029
CaTy-ai-O4′	In vacuo	81.283		230.234	344.407	51.983	0.4016
	In benzene	80.708		36.372	107.679	75.169	0.3863
	In acetonitrile	80.656		17.802	51.679	95.929	0.3643
	In water	82.057		5.113	29.794	104.015	0.3383
CaTy-ai-O4	In vacuo	72.003		220.954	321.770	65.339	0.2884
	In benzene	72.162		27.826	90.325	83.977	0.2821
	In acetonitrile	73.566		10.712	40.565	99.953	0.2738
	In water	76.001		−0.944	21.839	105.913	0.2630
CaD-ai-O4′	In vacuo	72.724	163.828	224.003	334.526	53.304	0.3396
	In benzene	72.794	144.587	30.347	64.901	74.899	
	In acetonitrile	73.787	129.406	11.333	81.390	94.483	0.3205
	In water	75.593	127.905	−0.560	26.091	101.254	0.3046
CaD-ai-O4	In vacuo	71.968		223.247	322.029	65.046	0.2884
	In benzene	72.152		29.705	90.471	83.821	0.2823
	In acetonitrile	73.565		11.112	40.586	99.932	0.2737
	In water	75.969		−0.1839	21.738	105.983	0.2632
CaD-aiii-O3′	In vacuo	72.925		224.595	334.447	53.584	0.3297
	In benzene	73.124		31.0284	99.219	76.045	0.32159
	In acetonitrile	74.553		12.199	45.665	95.841	0.311765
	In water	76.492		0.409	25.710	102.534	0.29506
CaD-aii-O3	In vacuo	75.017		226.329	326.791	63.333	0.3383
	In benzene	75.171		32.816	94.093	83.219	0.3298
	In acetonitrile	76.614		14.190	43.220	100.347	0.3189
	In water	78.889		2.711	23.889	106.751	0.3026
p-CoD-aii-O3′	In vacuo	72.893	164.937	223.525	333.926	54.074	0.3296
	In benzene	73.100	145.348	30.314	98.870	76.370	0.3220
	In acetonitrile	74.593	129.357	12.211	45.748	95.797	0.3119
	In water	76.756	127.937	0.548	26.116	102.393	0.2950
p-CoD-ai-O4′	In vacuo	72.787		230.570	329.476	65.570	0.3397
	In benzene	72.818		36.601	96.923	84.605	0.3317
	In acetonitrile	73.711		17.392	45.832	100.894	0.3207
	In water	75.804		5.337	25.630	107.667	0.3049

Table 2 continued

Structure	Media	BDE (kcal/mol)	IP (kcal/mol)	PDE (kcal/mol)	PA (kcal/mol)	ETE (kcal/mol)	Spin density on the radicalised O
p-CoD-aii-O4	In vacuo	79.939		230.066	330.051	64.952	0.3269
	In benzene	79.387		36.154	97.271	84.231	0.3139
	In acetonitrile	79.773		17.298	45.811	100.843	0.2947
	In water	81.545		5.274	25.582	107.629	0.2730
p-CoD-ai-O4	In vacuo	79.896		222.957	334.663	53.231	0.3261
	In benzene	79.362		29.610	99.745	75.213	0.3137
	In acetonitrile	79.702		11.307	46.097	94.567	0.2946
	In water	81.459		−0.382	26.165	101.390	0.2731
CiD-aii-O3′	In vacuo	72.969	169.134	219.394	333.795	54.280	0.3301
	In benzene	73.171	148.208	27.513	98.747	76.565	0.3223
	In acetonitrile	74.584	129.562	12.097	45.703	95.834	0.3122
	In water	76.645	127.758	0.653	26.029	102.367	0.2953
CiD-ai-O4′	In vacuo	72.864		218.837	334.248	53.723	0.3400
	In benzene	72.895		26.827	98.520	76.516	0.3320
	In acetonitrile	73.239		10.629	45.735	94.457	0.3135
	In water	75.830		−0.176	25.712	101.87	0.3052

position of the OH groups present. The IP values of *p*-CoD and that of CiD are greater (≈1 kcal/mol) than those of CaTy and CaPEA, respectively, which suggests that when the aromatic amine moiety is of catecholic nature, the resulting phenolic acid amide is a better electron donor than the phenolic acid amide in which the phenolic acid moiety has a catecholic nature. This result is consistent with the results obtained on dopamine and caffeonic acid (Table S1), which shows that dopamine is a better electron donor than caffeonic acid. The preference for dopamine as a better electron donor may be related to the fact that the lone pair of electrons on N (present in dopamine) is readily available for donation than the lone pair of electrons on the O atom (present in the carbonyl group of caffeonic acid). The IP values for CaD, *p*-CoD and CaTy are lower than those of quercetin and taxifolin (170.3 and 183.4 kca/mol, respectively, obtained with the same calculation method, [75]), suggesting that phenolic acid amides have the ability to scavenge radical species through the ET mechanism.

In solution, the IP value of each compound decreases with the increase in solvent polarity, which implies that the ability of the compounds to act through SET mechanism is enhanced with the increase in solvent polarity. A comparison across media also suggests that as the polarity increases, the IP value changes minimally across structures, so that in the most polar solvent, the IP value of all the compounds has the same value of ~128 kcal/mol.

The resonance structures of the cation free radicals obtained from the electron abstraction can be observed from the distribution of the atomic spin densities for CaD, *p*-CoD, CaTy, CiD and CaPEA. Figure 4 shows the distribution of atomic spin densities for the cation free radicals for these compounds. The calculated spin density for the electron abstraction from CaD shows a global contribution of 0.208 for the oxygen of the OH groups, 0.351 for the global contributions of ring X, 0.178 for the global contributions of the aliphatic chain and 0.263 for the global contributions of ring Y. *p*-CoD shows a global spin density contributions of 0.189 for oxygen of the OH groups, a 0.367 for the global spin density contributions in ring X, a 0.225 for the global spin density contributions in aliphatic chain and a 0.238 global spin contribution for ring Y. The data for CaTy, which is a structural isomer of *p*-CoD, shows a global spin density contribution of 0.016 for oxygen of the OH groups, a 0.035 decrease in global spin density contributions in ring X, a 0.007 reduction in global spin density contributions in aliphatic chain and an increase of 0.031 for the global spin contribution of ring Y. An assessment of the spin density of the N atom in the cation radical species may provide an indication on their relative stability. The order of the spin density distribution on the N atom is such that CaD < *p*-CoD < CiD ~CaTy < CaPEA, which is close to the trend in the IP values. Therefore, the lowest localisation of the unpaired electron on the N atom may explain the highest stability of CaD cation radical when compared to the other phenolic acid amides studied in this work.

A comparison of the IP values of the separate aromatic amine moiety with the corresponding phenolic acid moiety (e.g. caffeonic acid with dopamine and coumaric acid with tyramine, Table S1) suggests that aromatic amines are better electron donor than the phenolic acids. The preference

for the aromatic amines to donate electrons may be related to the presence of the N atom in the amine group. The N atom has greater tendency to donate electrons than the O atom in the C=O of phenolic acids.

The single electron transfer followed by proton transfer (SET-PT) mechanism

The formation of radical cations, in the first step of the SET-PT mechanism, requires an energy expense (kcal/mol) of 164–171 *in vacuo*, 145–149 in benzene, 129–130 in acetonitrile and 127–129 in water (IP values, Table 2). The PDE parameter characterises the second step of the SET-PT mechanism. The data in Table 2 indicate that *in vacuo*, the loss of the proton from the $ArOH^{\cdot+}$ requires even greater energy than the electron transfer reaction because the PDE values are higher than the IP values. The high values of PDE in vacuum suggest that this mechanism is not preferred. However, in different solvents the PDE value is significantly lower than the IP value. Therefore, it is reasonable to infer that in solution, the PT transfer reaction is thermodynamically preferred to the ET reaction. The preference for the PT reaction increases with the increase in solvent polarity.

Among the isolated aromatic amine and phenolic acid compounds (Table S1), electron-donating mechanism is also preferred *in vacuo*, while the loss of the proton is preferred in solvent media. A comparison of the PDE value, among the isolated aromatic amines and phenolic acids, suggests that it is lower for the aromatic amines than for the phenolic acid amides for the situation *in vacuo*, and it is lower for the phenolic acids than for the aromatic amines in other media.

Sequential proton loss electron transfer (SPLET) mechanism

The anions resulting from the loss of the proton are shown in Fig. S2, and their relative energies are reported in Table 1. In CaPEA and CaTy, where the catecholic unit is on ring X, the deprotonation of the 4-OH group yields to the most stable anion that is characterised by an internal H-bond. In CaTy, the deprotonation on the 4′-OH position results in significantly unpopulated anionic conformer. The energetic gaps among the anionic species of CaPEA and CaTy decrease with the increase in solvent polarity. In *p*-CoD and CiD, where the catecholic unit is on ring Y, the deprotonation of the OH group yields conformers whose energetics are not significantly different, both *in vacuo* and in different solvents. These latter results indicate that all the anions of *p*-CoD and CiD may coexist in vivo. In CaD, the only significant anionic conformer is the one in which the deprotonation occurs at the 4-OH group.

The SPLET mechanism is better described through the use of the PA and ETE parameters. The data for these parameters are reported in Table 2. The first step in the SPLET mechanism is proton loss, and it is determined by the acidity of the OH group. The PA values for all investigated compounds decrease with an increase in solvent polarity, which suggests that the proton loss reaction is least preferred *in vacuo* and best preferred in polar medium. Electron transfer from the phenoxide ion represents the second step in SPLET mechanism. This step is better discussed in terms of the electron transfer enthalpy (ETE). The ETE values increase with the increase in solvent polarity. In comparison with the PA values, the ETE values are significantly lower in non-polar media (*in vacuo* and in benzene) and higher in acetonitrile and water than the PA values. These results suggest that the electron transfer reaction from phenoxide anions to free radical species is thermodynamically preferred in non-polar media, while the proton loss reaction is thermodynamically preferred in acetonitrile and in water. These results also imply that the first step (the dissociation of the phenolic antioxidant into phenoxide anion form and a proton) is the rate-determining step *in vacuo* and in benzene (non-polar media), while the electron transfer mechanism is the rate-determining step in acetonitrile and in water. The second step (that involves a single-electron transfer) is a significant step for electron-deficient radical scavenging. The phenoxide anions derived from polyphenols are better electron donors and radical scavengers than the parent molecules. Low ETE value means deep extent of the radical-scavenging reaction. Therefore, although the first step of the SPLET mechanism is the rate-determining step *in vacuo* and in benzene, the extent of radical scavenging is determined by the second step.

A comparison of the PA and ETE parameters for the isolated aromatic amine and the corresponding phenolic acid (e.g. caffeonic acid and dopamine, coumaric acid and tyramine, Table S1) suggests that, in all the media, the PA value is lower for the phenolic acid than for the corresponding aromatic amine, while the ETE value is lower for the aromatic amine than for the corresponding phenolic acid. It is therefore reasonable to consider that aromatic amines are thermodynamically better radical scavenger than phenolic acids through the SPLET mechanism.

Thermodynamically preferred radical-scavenging mechanism

The preference for a particular reaction mechanism depends on both the solvent and properties of the radical species involved in the reaction [76–78]. To investigate the preferred mechanism of action for the radical scavenging,

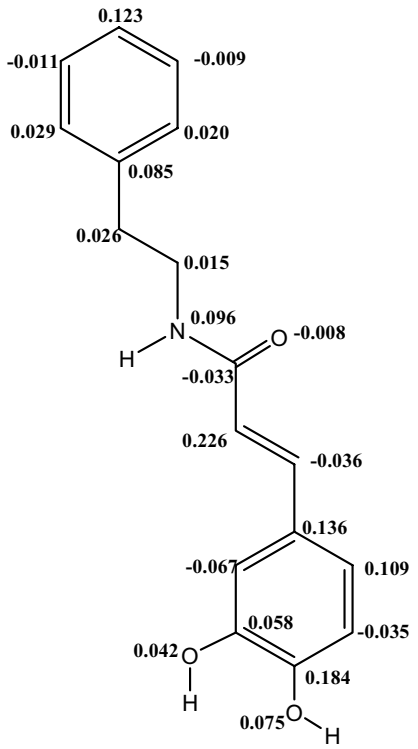

CaPEA

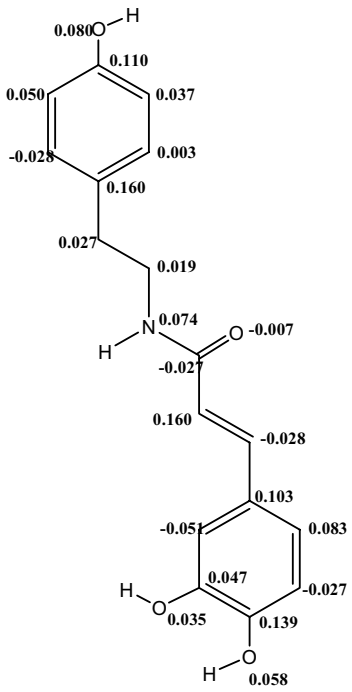

CaTy

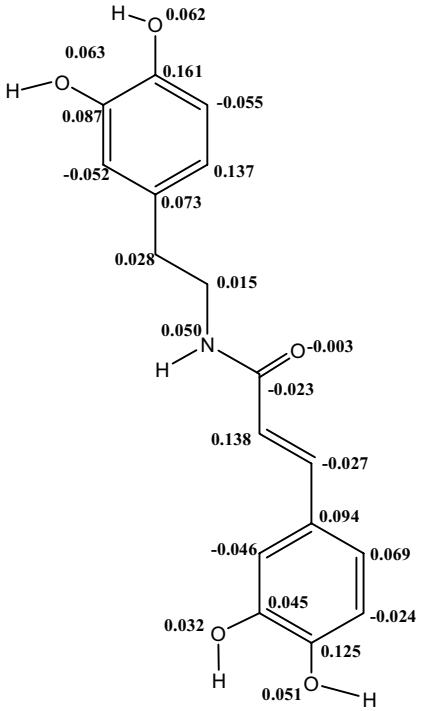

CaD

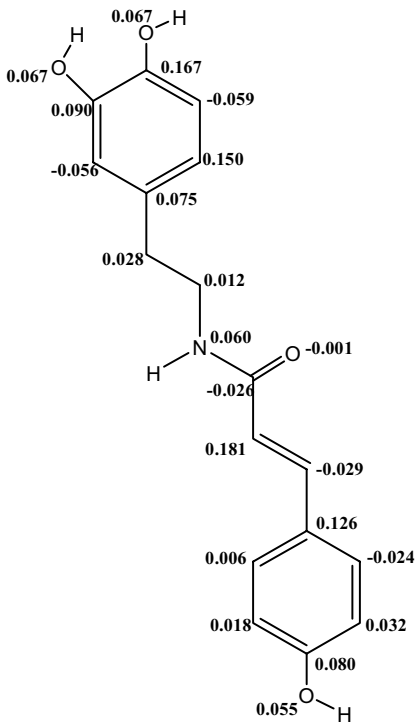

p-CoD

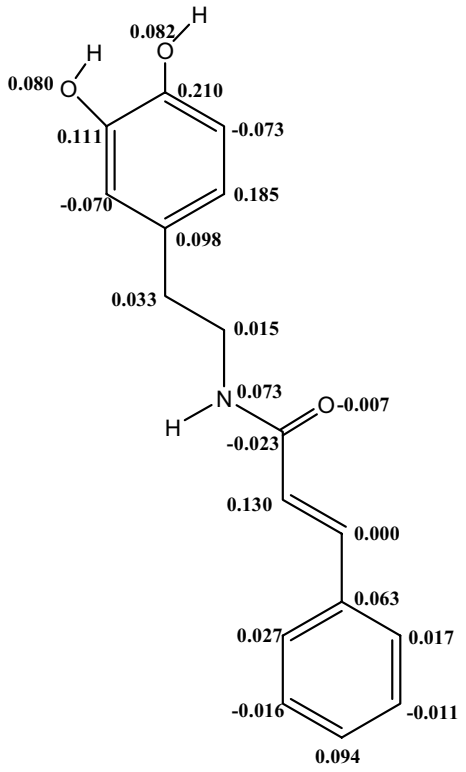

CiD

◀**Fig. 4** Atomic spin densities in the cation free radical species of the studied phenolic acid amide derivatives, B3LYP/6-311+G(d,p) results in vacuo for the lowest-energy conformer of each structure

it is necessary to compare the enthalpy values for the different processes. Because the calculated gas-phase ionisation potentials (IPs) and proton affinities (PAs) are significantly higher than phenolic O–H BDEs, it is reasonable to infer that that O–H bond dissociation represents the most probable process in the gas phase. The preference for the HAT mechanism in non-polar solvents may be related to the fact that it does not involve charge separation processes. The SET-PT mechanism is preferred in polar media due to the charge separation process [79]. The trend observed for the phenolic acid amides is also reproduced by the isolated phenolic acids and aromatic amine derivatives (Table S1). A comparison of the enthalpy values of the separate phenolic acids and aromatic amides with those of the phenolic acid amides clearly shows the preference for phenolic acid amides to act as radical scavengers.

Metal chelation mechanism: results of the study in vacuo

Acidities in the gas phase and in solution

Metal chelation mechanism often is a result of metal interacting with deprotonated hydroxyl in the polyphenolic compounds such as flavones [54]. The acidity values describe the ability of a molecule to lose a proton, $\Delta H_{\text{acidity}}$ is associated with the ability of molecule to lose proton *in vacuo*, and $\Delta G_{\text{acidity}}$ is associated with the ability of the molecule to lose a proton in solution. Both $\Delta H_{\text{acidity}}$ and $\Delta G_{\text{acidity}}$ values are reported in Table S3; they are generally higher than both BDE and the IP values (Table 2), indicating that the metal chelation mechanism is less preferred. Although this mechanism is minor with respect to radical-scavenging mechanisms, it is interesting to investigate how it occurs by determining the preferred complexes of Cu(II) with the phenolic acid amides. In this study, CaD molecule has been selected for the investigation because it combines the catecholic units on both aromatic amine and phenolic acid moieties.

Stability of the CaD···Cu^{2+} and the preferred binding sites for the Cu^{2+} ion

The calculated CaD···Cu^{2+} complexes are shown in Fig. 5. The relative energies (ΔE) and binding energies ($\Delta E_{\text{binding}}$) for the complexes, CaD···Cu bond distances, natural atomic charge Cu ion and the spin density of Cu ion in the complexes are reported in Table 3. The complexes are named in such a way that the name includes the original name of the starting structure (CaD), the symbol Cu for the cation and the Roman numbers indicating the possible site for Cu chelation on the CaD molecule. In principle, there are six possible sites on CaD for the Cu(II) chelation: two catechol moieties, two aromatic rings, the C=O group and the C=C double bond in the aliphatic chain. The coordination to these sites can give rise to six different complexes shown in Fig. 5.

In the lowest-energy complex, Cu(II) ion tri-dentated to CaD through both the oxygen atom of the C=O carbonyl group (1.869 Å) and the aromatic ring X through the atoms C1′ and C6′. The second lowest-energy complex (CaD···Cu-IV) is 14.247 kcal/mol above the lowest-energy complex structure. In this structure, the Cu ion is bi-dentated to CaD through the O atom of the C=O carbonyl group and the H7 atom. The rest of the complexes have relative energies >19 kcal/mol, which is an indication that these configurations are not preferred. The highest-energy complexes are those in which the Cu ion is coordinated through the benzene ring of each of the catechol unit, with the Cu ion preferring to bind through the X ring than the Y ring. The relative energy values of the last four complexes indicates that Cu(II) has poor chelating power towards both the catechol group and the benzene ring.

Because of the acidic nature of the OH groups in these compounds, it is possible to consider that these compounds may exist in some anionic form at physiological pH values. It was therefore considered interesting to study the interaction between the Cu(II) ion and some of the anionic forms of CaD. The Cu(II) cation may attack not only the deprotonation sites but also the other positions that are electron-rich centres. The investigated structures are shown in Fig. 6, and their relative energies and binding energies are reported in Table 3. The results of the study show that the Cu ion prefers to bind simultaneously to both the carbonyl O atom and the aromatic ring Y (through the π electrons of the aromatic ring). All other configurations of $(\text{CaD}\cdots\text{Cu})^{+}$ have relatively high energy to be considered populated.

The binding energy ($\Delta E'_{\text{binding}}$), at different chelation sites, informs about the metal ion affinity (MIA) and also the preferred site on CaD for interaction with the metal cation. The trends in the $\Delta E'_{\text{binding}}$ follow the same trend as the stabilisation energies. In this way, the MIA is highest when the Cu^{2+} cation is simultaneously chelated on the π system of aromatic ring Y and the lone pair of electrons of the O atom of the carbonyl group. A comparison of the $\Delta E'_{\text{binding}}$ between the neutral complexes and the deprotonated complexes suggests that $\Delta E'_{\text{binding}}$ is higher among the complexes with the deprotonated CaD-ai than those with the neutral CaD.

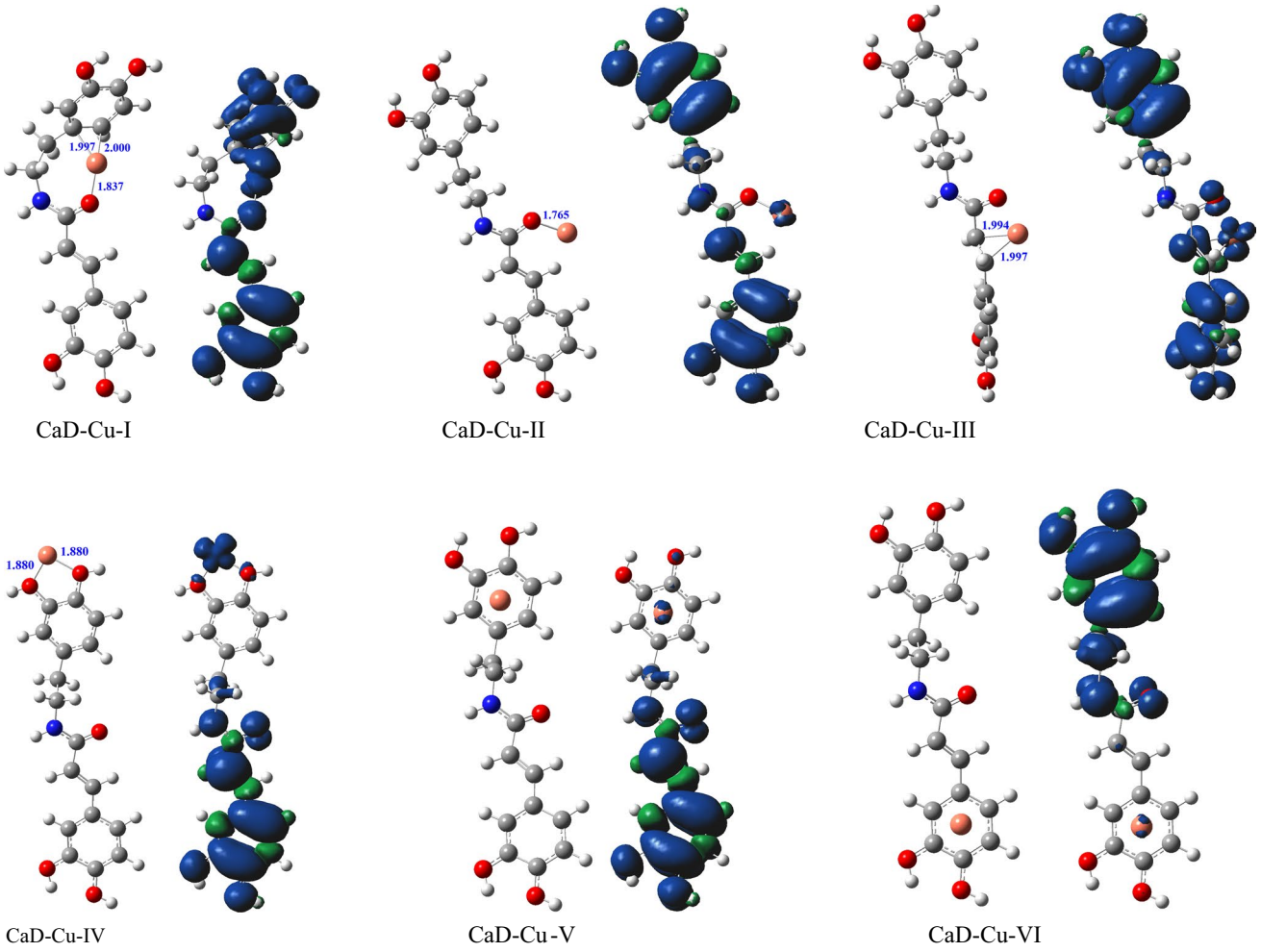

Fig. 5 Optimised structures and spin density distribution on the CaD···Cu complexes, B3LYP/6-311+G(d,p) results *in vacuo*. Representative CaD···Cu bond distances (Å) are indicated in *blue* colour

AIM analysis, NPA charges and spin density in the Cu^{2+}···ligand complexes

The topology of the electron density distribution $\rho(r)$, its first derivative $\nabla\rho(r)$ and second derivative (Laplacian) $\nabla\rho(r)$ provides information about the electronic structure of a molecule. Both electron density and electron energy density (H), obtained from the AIM analysis, at the different bond critical points (BCP), are often utilised to characterise and determine the strength of a given bond [80–82]. The relation between the electron density at BCP and the bond strength has been found for strong bonds (e.g. covalent bonds), and for weak interactions, such as metal–ligand interactions and hydrogen bonding [83–86]. Also, the values H and its components, the kinetic (G) and potential (V) electron energy densities provide valuable information on the nature of the chemical bond. For the strongest bonds, such as covalent bonds, V is usually negative and relatively large, G is positive, and H is negative. In such systems, both interacting atoms are sharing electrons, which are considerably localised in the internuclear space between the atoms of interest. The potential energy density estimated in BCP has large values because the electrons are relatively stable energetically in the internuclear region. Strong bonds are characterised by negative values of $\nabla^2\rho$ and are referred to as shared interactions. Weak bonds, such as H-bonding interactions, are characterised as closed-shell interactions. In this type of bonding, H has positive value and is close to zero, G has positive value, and V has negative value. However, the positive value of G predominates over the negative value of V, since the electrons are energetically less stable in the region between two closed-shell systems. Closed-shell interactions are also accompanied by positive values of $\nabla^2\rho$ estimated at the corresponding BCP, around which the electron density is depleted. The metal–ligand interaction has characteristics that represent the mix of shared and closed-shell interactions. For instance, the value of H is usually negative and close to zero, as found for shared

Table 3 CaD···Cu bond distance, relative energies (ΔE, kcal/mol), interaction energy (ΔE_{inter}, kcal/mol), spin density and charge on the Cu ion (obtained from NPA analysis) for the complexes of CaD and Cu ion, B3LYP/6-311+G(3df,2p)//B3LYP/6-311+G(d,p) results *in vacuo*

Complexes	Bond type	Bond distance (Å)	ΔE (kcal/mol)	$\Delta E_{binding}$ (kcal/mol)	Spin density	Charge on Cu (*e*)
Neutral form of CaD						
CaD···Cu-I	C1′–Cu	1.997	0.000	366.524	0.1337	0.958
	C6′–Cu	2.000				
	O9–Cu	1.837				
CaD···Cu-II	O9–Cu	1.765	14.247	352.276	−0.0003	0.852
	H7–Cu	1.899				
CaD···Cu-III	C7–Cu	1.997	19.055	347.469	0.0651	1.057
	C8–Cu	1.994				
	O9–Cu	1.986				
CaD···Cu-IV	O3′–Cu	1.880	23.681	346.487	0.0996	0.954
	O4′–Cu	1.880				
CaD···Cu-V	C1′–Cu	2.117	28.441	338.083	0.0078	0.859
	C2′–Cu	2.095				
	C5′–Cu	2.102				
	C6′–Cu	2.091				
CaD···Cu-VI	C1–Cu	2.142	31.348	335.176	0.0044	0.858
	C2–Cu	2.095				
	C5–Cu	2.103				
	C6–Cu	2.095				
Anionic form of CaD						
CaD-an-O4···Cu-I	C1′–Cu	1.979	0.000	518.152	0.0085	0.876
	C6′–Cu	1.970				
	O9–Cu	1.837				
CaD-an-O4···Cu-II	O3–Cu	1.950	22.489	507.389	0.2226	0.935
	O4–Cu	1.798				
CaD-an-O4′···Cu-III	O3′–Cu	1.957	23.038	519.522	0.2409	0.942
	O4′–Cu	1.794				
CaD-an-O3′···Cu-IV	O3′–Cu	1.796	24.055	518.811	0.2727	0.957
	O4′–Cu	1.942				
CaD-an-O3···Cu-V	O3–Cu	1.796	25.748	512.037	0.2750	0.956
	O4–Cu	1.939				
CaD-an-O4···Cu-VI	C7–Cu	1.963	29.025	489.127	0.1137	1.009
	C8–Cu	2.028				
	O9–Cu	1.964				

interactions, but with a positive value of $\nabla^2\rho$, as found for closed-shell interactions [87].

The bond critical point data for the studied CaD···Cu complexes are reported in Table 4. The largest value of ρ corresponds to Cu^{2+}···O9 bond, indicating that this is the strongest site at which the metal ion interacts with the ligand. Therefore, the strongest inter-atomic interaction corresponds to the situation in which the M^{2+} ion is bonded to the sp^2 O atom. This result is in agreement with the fact that the sp^2 O has the highest available lone pair of electrons than other electron donor centres present in the molecule.

The value of H is always negative and close to zero with a range of 0.009–0.056, indicating closed-shell interaction. The ratio $|V|/G$ is utilised to characterise a chemical bond; interactions with $|V|/G < 1$ are characteristic of closed-shell interactions; interactions with $|V|/G > 2$ are typically shared interactions; and interactions with $1 < |V|/G < 2$ represent interactions of intermediate character [88, 89]. The results reported in Table 4 show that the CaD···Cu interactions have a range of 1.2–1.61, what is indicative of intermediate between covalent and ionic character. The values of $\nabla^2\rho$ are positive, indicative of a predominantly closed-shell (ionic) interaction. This means that although the interactions are

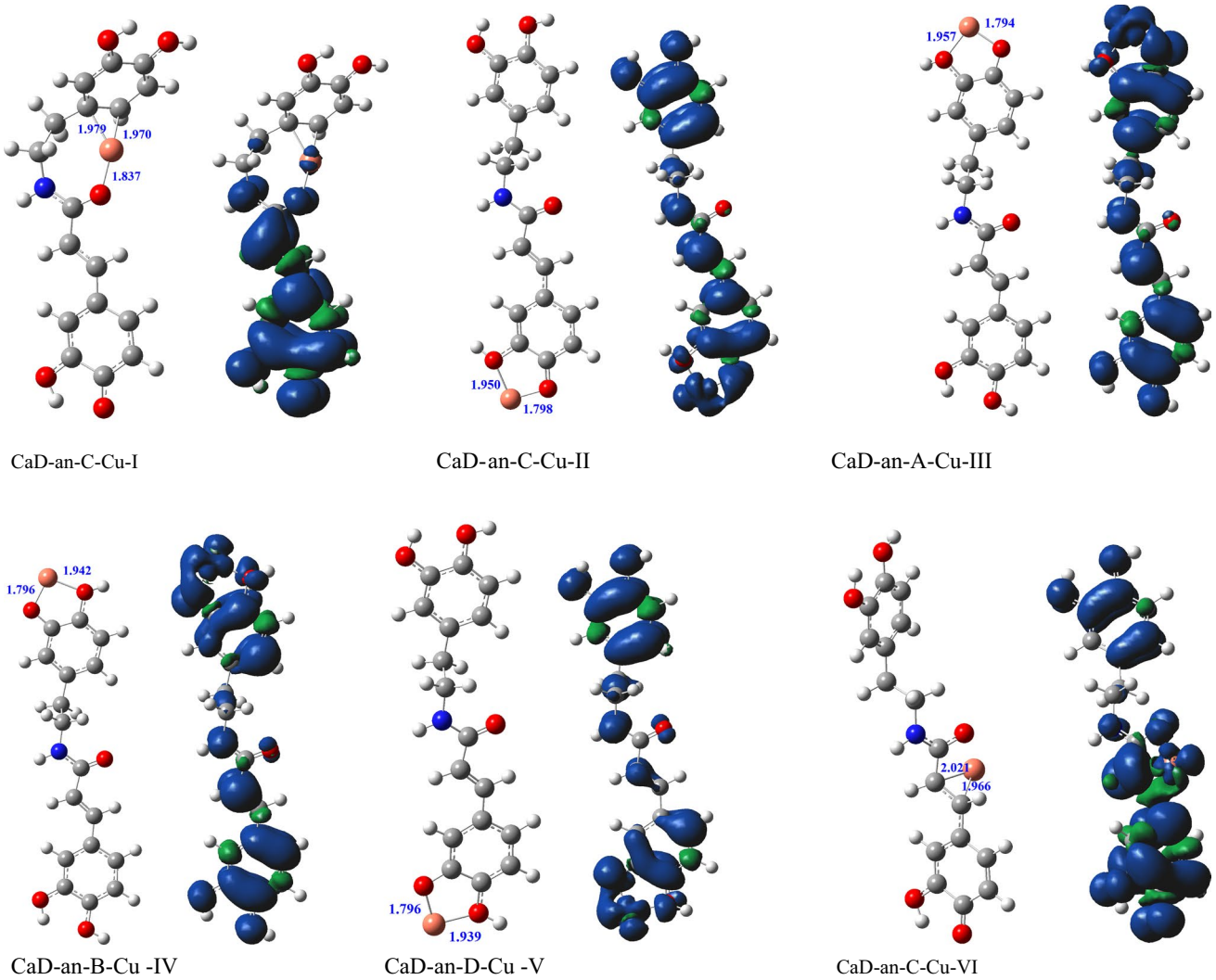

Fig. 6 Optimised structures and spin density distribution on the CaD···Cu complexes for the deprotonated ligand, B3LYP/6-311+G(d,p) results in vacuo. Representative CaD···Cu bond distances (Å) are indicated in *blue* colour

intermediate between covalent and ionic character, they are more inclined towards ionic character.

The free Cu(II) cation has a charge of +2. The charge on the Cu(II) ion in the complexes with CaD (reported in Table 3) has the range of 0.852–1.057*e*. These results suggest that on interaction with CaD, the Cu(II) ion is reduced to Cu(I) ion. In the process, CaD is oxidised so that the complexes that are obtained with the copper ion are of the form $[CaD\cdots Cu]^{+}$. The spin density of Cu(II) ions in the isolated state is 1 and for the neutral CaD ligand is zero. The atomic spin density of Cu ion in the complex has the range of 0.0003–0.1337 for the situation in which the Cu ion binds to the neutral CaD molecule and a range of 0.0085–0.2750 for a situation in which the Cu ion binds to the anionic species. In both situation, therefore, the Cu(II) tends to have significantly small spin density with respect to the isolated Cu(II) ion.

Metal chelation mechanism in the presence of water solvent

The polarisation effects of the solvent molecules, on both the geometries and energies of the complexes of CaD with Cu^{2+} ions, were taken into account through using the PCM, SMD model. The relative energy (ΔE_{soln}), binding energy ($\Delta E_{inter,soln}$), charges and spin densities on the Cu^{2+} ions are reported in Table S4; the bond critical point data are reported in Table S5. The geometries of the complexes are similar between the results *in vacuo* and the results in water solution. However, the CaD···Cu^{2+} bond distance is longer in water solution than *in vacuo*, indicating that the interaction between the ligand and the M^{2+} ion is stronger *in vacuo* than in solution. The relative energy order of the complexes in water solution is not significantly different from the order of the relative energies of the complexes *in vacuo*.

Table 4 Bond critical point data for the CaD···Cu complexes, result of the study *in vacuo*

Complexes	Bond type	ρ (Hartree)	$\nabla^2\rho$ (Hartree)	V (Hartree)	G (Hartree)	H (Hartree)	$\frac{\lvert V\rvert}{G}$
Neutral form of CaD							
CaD···Cu-I	C1′–Cu	0.096	0.149	−0.139	0.088	−0.051	1.579
	C6′–Cu	0.096	0.153	−0.139	0.089	−0.051	1.570
	O9–Cu	0.116	0.592	−0.225	0.186	−0.039	1.207
CaD···Cu-II	O9–Cu	0.136	0.808	−0.281	0.242	−0.040	1.164
	H7–Cu	0.044	0.107	−0.046	0.036	−0.009	1.260
CaD···Cu-III	C7–Cu	0.095	0.169	−0.142	0.092	−0.050	1.543
	C8–Cu	0.097	0.165	−0.145	0.093	−0.052	1.557
	O9–Cu	0.085	0.341	−0.147	0.116	−0.031	1.266
CaD···Cu-IV	O3′–Cu	0.100	0.507	−0.195	0.161	−0.034	1.212
	O4′–Cu	0.101	0.509	−0.195	0.161	−0.034	1.211
CaD···Cu-V	C1′–Cu	0.072	0.202	−0.103	0.077	−0.026	1.342
	C2′–Cu	0.075	0.183	−0.109	0.077	−0.031	1.408
	C5′–Cu	0.074	0.195	−0.108	0.078	−0.029	1.376
	C6′–Cu	0.075	0.200	−0.110	0.080	−0.030	1.377
CaD···Cu-VI	C1–Cu	0.068	0.208	−0.096	0.074	−0.022	1.298
	C2–Cu	0.075	0.175	−0.108	0.076	−0.032	1.424
	C5–Cu	0.074	0.195	−0.108	0.078	−0.029	1.376
	C6–Cu	0.074	0.197	−0.109	0.079	−0.030	1.377
Anionic form of CaD							
CaD-an-O4···Cu-I	C1′–Cu	0.100	0.155	−0.148	0.093	−0.055	1.585
	C6′–Cu	0.102	0.161	−0.153	0.097	−0.056	1.584
	O9–Cu	0.116	0.597	−0.226	0.187	−0.038	1.204
CaD-an-O4···Cu-II	O3–Cu	0.086	0.378	−0.155	0.125	−0.031	1.244
	O4–Cu	0.131	0.699	−0.263	0.219	−0.044	1.201
CaD-an-O4′···Cu-III	O3′–Cu	0.085	0.368	−0.152	0.122	−0.030	1.246
	O4′–Cu	0.133	0.710	−0.267	0.222	−0.045	1.201
CaD-an-O3′···Cu-IV	O3′–Cu	0.132	0.696	−0.263	0.219	−0.045	1.204
	O4′–Cu	0.088	0.391	−0.159	0.129	−0.031	1.240
CaDi-an-O3···Cu-V	O3–Cu	0.132	0.693	−0.262	0.218	−0.045	1.205
	O4–Cu	0.088	0.395	−0.160	0.130	−0.031	1.237
CaD-an-O4···Cu-VI	C7–Cu	0.101	0.147	−0.151	0.094	−0.057	1.608
	C8–Cu	0.091	0.199	−0.138	0.094	−0.044	1.471
	O9–Cu	0.089	0.365	−0.157	0.124	−0.033	1.265

All the complexes in solution have $\Delta E'_{\text{binding,soln}} > 0$, indicating that Cu^{2+} has a tendency to bind to CaD. Among the lowest-energy complexes, the binding energy decreases significantly with respect to the binding energy obtained *in vacuo*, what suggests that CaD has less affinity for the Cu^{2+} ion in water than *in vacuo*. The decreased affinity of the ligand towards the metal ion may be related to the presence of polarisation effects in solution, which are absent *in vacuo* [29].

The spin density values have a range of 0.2424–0.7472. In comparison with the results *in vacuo*, the spin density on the Cu^{2+} ion is less depleted in solution than *in vacuo*. The charge on the Cu^{2+} ion decreases less (1.241−1.610*e*) in comparison with the results *in vacuo*, indicating that the positive charge is less dissipated in solution. An analysis of the bond critical point data suggests that in solution, the O9···Cu bond is weak in solution than *in vacuo* because of having smaller value of ρ in solution than *in vacuo*. However, the trend in all other properties is the same as that *in vacuo*, suggesting intermediate type of bonding with greater inclination towards ionic character.

Conclusion

Theoretical studies on the antioxidant properties phenolic acid amides were performed to investigate factors that

contribute to their conformational preferences and to elucidate their antioxidant properties and mechanisms. The antioxidant activity has been considered through the ability of phenol acid amides to scavenge free radical species and through their ability to chelate metal ions.

The radical-scavenging activity has been investigated through the hydrogen atom transfer (HAT), the electron transfer mechanisms (ET), the single-electron transfer followed by proton transfer (SET-PT) and the sequential proton loss electron transfer mechanisms (SPLET). In general, the antioxidant activity through the HAT mechanism depends on the arrangement of hydroxyl substituents on the aromatic ring. The abstraction of the H atom from the phenolic OH group is preferred to the abstraction of the H atom from the NH group. Moreover, the abstraction of the H atom from the *para* OH group in a catecholic unit contributes the strongest strong free-radical-scavenging properties for the phenolic acid amides. Based on the calculated thermodynamic parameters, phenolic acid amides can be considered to be better radical scavenger than the isolated aromatic amines and phenolic acids.

The metal chelation properties of phenolic acid amides depend on the affinity of the Cu ion for the different binding sites.

The study suggests that the preferred complexation site for phenolic acid amides is the simultaneous binding to the carbonyl O atom and the benzene ring of the aromatic amide. An estimated metal ion affinity (MIA) is influenced by the nature of the ligand and the media; it is higher when the ligand associated with the metal ion is an anion than when it is a neutral molecule, and it is significantly lower in aqueous solution than *in vacuo*. The interaction of CaD with the Cu ion shows the ability of CaD to reduce the metal ions from a $+2$ state to a $+1$ state. An AIM analysis suggests that the CaD$\cdots$Cu interactions correspond to the mixed type interactions with greater inclination towards ionic character.

Conflict of interest The author declares that he has no competing interests.

Compliance with ethics requirements This article does not contain any studies with human or animal subjects.

References

1. Wang T, Gu J, Wu PF, Wang F, Xiong Z, Yang YJ, Wu WN, Dong LD, Chen JG (2009) Protection by tetrahydroxystilbene glucoside against cerebral ischemia: involvement of JNK, SIRT1, and NF-kappaB pathways and inhibition of intracellular ROS/RNS generation. Free Radic Biol Med 47:229–240
2. Krishnaiah D, Sarbatly R, Nithyanandam R (2011) A review of the antioxidant potential of medicinal plant species. Food Bioprod Process 89:217–233
3. Mwangi HM, Westhuizen JVD, Marnewick J, Mabusela WT, Kabanda MM, Ebenso EE (2013) Isolation, identification and radical scavenging activity of phlorotannin derivatives from brown algae, *Ecklonia maxima*: an experimental and theoretical study. Free Radic Antioxid 3:S1–S10
4. Kabanda MM, Mammino L, Murulana LC, Mwangi HM, Mabusela WT (2015) Antioxidant radical scavenging properties of phenolic pent-4-en-1-yne derivatives isolated from *Hypoxis rooperi*. A DFT study *in vacuo* and in solution. Int J Food Prop 18:149–164
5. Kranl K, Schlesier K, Bitsch R, Hermann H, Rohe M, Böhm V (2005) Comparing antioxidative food additives and secondary plant products—use of different assays. Food Chem 93:171–175
6. Jennings BH, Akoh CC (2009) Effectiveness of natural versus synthetic antioxidants in a rice bran oil-based structured lipid. Food Chem 114:1456–1461
7. Aissa I, Sghair RM, Bouaziz M, Laouini D, Sayadi S, Gargouri Y (2012) Synthesis of lipophilic tyrosyl esters derivatives and assessment of their antimicrobial and antileishmania activities. Lipids Health Dis 11:1
8. Trabelsi N, Oueslati S, Ksouri R, Nassra M, Marchal A, Krisa S, Abdelly C, Mérillon J-M, Waffo-Téguo P (2014) The antioxidant properties of new dimer and two monomers of phenolic acid amides isolated from *Limoniastrum guyonianum*. Food Chem 146:466–471
9. Yamamoto I, Matsunaga T, Kobayashi H, Watanabe K, Yoshimura H (1991) Analysis and pharmacotoxicity of feruloyltyramine as a new constituent and p-coumaroyltyramine in *Cannabis sativa* L. Pharmacol Biochem Behav 40:465–469
10. Marinova E, Georgiev L, Totseva I, Seizova K, Milkova T (2013) Antioxidant activity and mechanism of action of some synthesised phenolic acid amides of aromatic amines. Czech J Food Sci 31:5–13
11. Park JB (2009) Isolation and characterization of N-feruloyltyramine as the P-selectin expression suppressor from garlic (*Allium sativum*). J Agric Food Chem 57:8868–8872
12. Choi J-Y, Kim H, Choi Y-J, Ishihara A, Back K, Lee S-G (2010) Cytoprotective activities of hydroxycinnamic acid amides of serotonin against oxidative stress-induced damage in HepG2 and HaCaT cells. Fitoterapia 81:1134–1141
13. Son S, Lewis BA (2002) Free radical scavenging and antioxidative activity of caffeic acid amide and ester analogues: structure-activity relationship. J Agric Food Chem 50:468–472
14. Ley JP, Bertram H-J (2001) Synthesis of polyhydroxylated aromatic mandelic acid amides and their antioxidative potential. Tetrahedron 57:1277–1282
15. Yen G-C, Hsieh C-L (1997) Antioxidant effects of dopamine and related compounds. Biosci Biotechnol Biochem 61:1646–1649
16. Fresco P, Borges F, Diniz C, Marques MPM (2006) New insights on the anticancer properties of dietary polyphenols. Med Res Rev 26:747–766
17. Gaspar A, Garrido EM, Esteves M, Quezada E, Milhaze N, Garrido J, Borges F (2009) New insights into the antioxidant activity of hydroxycinnamic acids: synthesis and physicochemical characterization of novel halogenated derivatives. Eur J Med Chem 44:2092–2099
18. Gaspar A, Martins M, Silva P, Garrido EM, Garrido J, Firuzi O, Miri R, Saso L, Borges F (2010) Dietary phenolic acids and derivatives. Evaluation of the antioxidant activity of sinapic acid and its alkyl esters. J Agric Food Chem 58:11273–11280
19. Sellami M, Châari A, Aissa I, Bouaziz M, Gargouri Y, Miled N (2013) Newly synthesized dopamine ester derivatives and assessment of their antioxidant, antimicrobial and hemolytic activities. Process Biochem 48:1481–1487
20. Iuga C, Alvarez-Idaboy JR, Vivier-Bunge A (2011) ROS initiated oxidation of dopamine under oxidative stress

conditions in aqueous and lipidic environments. J Phys Chem B 115:12234–12246
21. Lucarini M, Pedulli GF (1994) Bond dissociation enthalpy of a-tocopherol and other phenolic antioxidants. J Org Chem 59:5063–5070
22. Marino T, Galano A, Russo N (2014) Radical scavenging ability of gallic acid toward OH and OOH radicals. Reaction mechanism and rate constants from the density functional theory. J Phys Chem B 118:10380–10389
23. Urbaniak A, Molski M, Szeląg M (2012) Quantum-chemical calculations of the antioxidant properties of *trans-p*-coumaric acid and *trans*-sinapinic acid. Comput Methods Sci Technol 18:117–128
24. Yeh YH, Lee YT, Hsieh HS, Hwang DF (2009) Dietary caffeic acid, ferulic acid and coumaric acid supplements on cholesterol metabolism and antioxidant activity in rats. J Food Drug Anal 17:123–132
25. Galano A, Francisco-Marquez M, Alvarez-Idaboy JR (2011) Mechanism and kinetics studies on the antioxidant activity of sinapinic acid. Phys Chem Chem Phys 13:11199–11205
26. Bakalbassis EG, Chatzopoulou A, Melissas VS, Tsimidou M, Tsolaki M, Vafiadis A (2001) Ab initio and density functional theory studies for the explanation of the antioxidant activity of certain phenolic acids. Lipids 36:181–191
27. Ley JP (2001) Phenolic acid amides of phenolic benzylamines against UVA-induced oxidative stress in skin. Int J Cosmet Sci 23:35–48
28. Kabanda MM, Tran VT, Seema KM, Serobatse KRN, Tsiepe TJ, Tran QT, Ebenso EE (2015) Conformational, electronic and antioxidant properties of lucidone, linderone and methyllinderone: DFT, QTAIM and NBO studies. Mol Phys 113:683–697
29. Kabanda MM (2012) Antioxidant activity of rooperol investigated through Cu(I and II) chelation ability and hydrogen transfer mechanism. A DFT study. Chem Res Toxicol 25:2153–2166
30. Mammino L, Kabanda MM (2009) A computational study of the effects of different solvents on the characteristics of the intramolecular hydrogen bond in acylphloroglucinols. J Phys Chem A 113:15064–15077
31. Mammino L, Kabanda MM (2009) A study of the intramolecular hydrogen bond in acylphloroglucinols. J Mol Struct (Theochem) 901:210–219
32. Kabanda MM, Mammino L (2012) A comparative study of the dimers of selected hydroxybenzenes. Int J Quantum Chem 112:519–531
33. Mammino L, Kabanda MM (2011) Interplay of intramolecular hydrogen bonds, OH orientations and symmetry factors in the stabilization of polyhydroxybenzenes. Int J Quantum Chem 111:3701–3716
34. Mammino L, Kabanda MM (2010) Adducts of acylphloroglucinols with explicit water molecules: similarities and differences across a sufficiently representative number of structures. Int J Quantum Chem 110:2378–2390
35. Mammino L, Kabanda MM (2010) Computational study of the carboxylic acid of phloroglucinol *in vacuo* and in water solution. Int J Quantum Chem 110:595–623
36. Mammino L, Kabanda MM (2008) A study of the interactions of the caespitate molecule with water. Int J Quantum Chem 108:1772–1792
37. Mammino L, Kabanda MM (2008) A computational study of the interactions of the phloroglucinol molecule with water. J Mol Struct (Theochem) 852:36–45
38. Mammino L, Kabanda MM (2007) Model structures for the study of acylated phloroglucinols and computational study of the caespitate molecule. J Mol Struct (Theochem) 805:39–52
39. Kabanda MM, Ebenso EE (2013) Structures, stabilization energies, and binding energies of quinoxaline···$(H2O)_n$, quinoxaline dimer, and quinoxaline···Cu complexes: a theoretical study. J Phys Chem A 117:1583–1595
40. Mammino L, Kabanda MM (2013) The role of additional O–H···O intramolecular hydrogen bonds for acylphloroglucinols' conformational preferences in vacuo and in solution. Mol Simul 39:1–13
41. Kabanda MM, Ebenso EE (2014) MP2, DFT and DFT-D study of the dimers of diazanaphthalenes: a comparative study of their structures, stabilisation and binding energies. Mol Simul 40:1131–1146
42. Kabanda MM, Ebenso EE (2013) DFT study of the protonation and deprotonation enthalpies of benzoxazole, 1,2-benzisoxazole and 2,1-benzisoxazole and implications for the structures and energies of their adducts with explicit water molecules. J Theor Comput Chem 12:1350070
43. Amorati R, Lucarini M, Mugnaini V, Pedulli GF (2003) Hydroxylamines as oxidation catalysts: thermochemical and kinetic studies. J Org Chem 68:1747–1754
44. Bel'kov MV, Ksendzova GA, Kuzovkov PV, Polozov GI, Skornyakov IV, Sorokin VL, Tolstorozhev GB, Shadyro OI (2007) Intramolecular hydrogen bonds and antioxidant activity of aminophenols. J Appl Spectrosc 74:635–641
45. Leopoldini M, Pitarch IP, Russo N, Toscano M (2004) Structure, conformation and electronic properties of apigenin, luteolin and taxifolin antioxidants. A first principle theoretical study. J Phys Chem A 108:92–96
46. Leopoldini M, Marino T, Russo N, Toscano M (2004) Antioxidant properties of phenolic compounds. H-atom versus electron transfer mechanism. J Phys Chem A 108:4916–4922
47. Leopoldini M, Marino T, Russo N, Toscano M (2004) Density functional computations of the energetic and spectroscopic parameters of quercetin and its radicals in the gas phase and in solvent. Theor Chem Acc 111:210–216
48. Sadasivam K, Kumaresan R (2011) A comparative DFT study on the antioxidant activity of apigenin and scutellarein flavonoid compounds. Mol Phys 109:839–852
49. Klein E, Lukeš V (2007) DFT/B3LYP study of the substituent effect on the reaction enthalpies of the individual steps of sequential proton loss electron transfer mechanism of phenols antioxidant action: correlation with phenolic C–O bond length. J Mol Struct (Theochem) 805:153–160
50. Musialik M, Litwinienko G (2005) Scavenging of dpph$^{\cdot}$ radicals by vitamin E is accelerated by its partial ionization: the role of sequential proton loss electron transfer. Org Lett 7:4951–4954
51. Huang D, Ou B, Prior RL (2005) The chemistry behind antioxidant capacity assays. J Agric Food Chem 53:1841–1856
52. Prior RL, Wu X, Schaich K (2005) Standardized methods for the determination of antioxidant capacity and phenolics in foods and dietary supplements. J Agric Food Chem 53:4290–4302
53. Kumar KS, Kumaresan R (2013) Theoretical investigation of the conformational, electronic and antioxidant properties of azaleatin, isorhamnetin and quercetagetin. Mol Simul 39:72–83
54. Leopoldini M, Russo N, Chiodo S, Toscano M (2006) Iron chelation by the powerful antioxidant flavonoid quercetin. J Agric Food Chem 54:6343–6351
55. Alcaro S, Chiodo SG, Leopoldini M, Ortuso F (2013) Antioxidant efficiency of oxovitisin, a new class of red wine pyranoanthocyanins, revealed through quantum mechanical investigations. J Chem Inf Model 53:66–75
56. Marković Z, Đorović J, Dekić M, Radulović M, Marković S, Ilić M (2013) DFT study of free radical scavenging activity of erodiol. Chem Pap 67:1453–1461
57. Alfaro RAD, Gomez-Sandoval Z, Mammino L (2014) Evaluation of the antiradical activity of hyperjovinol-A utilizing donor-acceptor maps. J Mol Model 20:2337
58. Rong YZ, Wang ZW, Zhao B (2013) DFT-based quantum chemical studies on conformational, electronic and antioxidant

properties of isobavachalcone and 4-hydroxyderricin. Food Biophys 8:250–255
59. Marenich AV, Cramer CJ, Truhlar DG (2009) Universal solvation model based on solute electron density and on a continuum model of the solvent defined by the bulk dielectric constant and atomic surface tensions. J Phys Chem B 113:6378–6396
60. Lamsabhi AM, Alcamí M, Mó O, Yáñez M (2006) Gas-phase deprotonation of uracil–Cu^{2+} and thiouracil–Cu^{2+} complexes. J Phys Chem A 11:1943–1950
61. Lamsabhi AM, Alcamí M, Mó O, Yáñez M (2003) Gas-phase reactivity of uracil, 2-thiouracil, 4-thiouracil, and 2,4-dithiouracil towards the Cu^{+} cation: a DFT study. ChemPhysChem 4:1011–1016
62. Lamsabhi AM, Alcamí M, Mó O, Yáñez M, Tortajada J, Salpin J-Y (2007) Unimolecular reactivity of uracil–Cu(2+) complexes in the gas phase. ChemPhysChem 8:181–187
63. Lamsabhi AM, Alcamí M, Mó O, Yáñez M, Tortajada J (2004) Association of Cu^{2+} with uracil and its thio derivatives: a theoretical study. ChemPhysChem 5:1871–1878
64. Alagona G, Ghio C (2009) Antioxidant properties of pterocarpans through their copper(II) coordination ability. A DFT study in vacuo and in aqueous solution. J Phys Chem A 113:15206–15216
65. Alagona G, Ghio C (2009) Plicatin B conformational landscape and affinity to copper (I and II) metal cations. A DFT study. Phys Chem Chem Phys 11:776–790
66. Frisch MJ, Trucks GW, Schlegel HB, Scuseria GE, Robb MA, Cheeseman JR, Scalmani G, Barone V, Mennucci B, Petersson GA, Nakatsuji H, Caricato M, Li X, Hratchian HP, Izmaylov AF, Bloino J, Zheng G, Sonnenberg JL, Hada M, Ehara M, Toyota K, Fukuda R, Hasegawa J, Ishida M, Nakajima T, Honda Y, Kitao O, Nakai H, Vreven T, Montgomery JA Jr, Peralta JE, Ogliaro F, Bearpark M, Heyd JJ, Brothers E, Kudin KN, Staroverov VN, Kobayashi R, Normand J, Raghavachari K, Rendell A, Burant JC, Iyengar SS, Tomasi J, Cossi M, Rega N, Millam JM, Klene M, Knox JE, Cross JB, Bakken V, Adamo C, Jaramillo J, Gomperts R, Stratmann RE, Yazyev O, Austin AJ, Cammi R, Pomelli C, Ochterski JW, Martin RL, Morokuma K, Zakrzewski VG, Voth GA, Salvador P, Dannenberg JJ, Dapprich S, Daniels AD, Farkas O, Foresman JB, Ortiz JV, Cioslowski J, Fox DJ (2009) Gaussian 09, Revision D.01. Gaussian Inc, Wallingford
67. Foster JP, Reed AE, Carpenter JE, Weinhold F (1980) Natural hybrid orbitals. J Am Chem Soc 102:7211–7218
68. Reed AE, Curtiss LA, Weinhold F (1988) Intermolecular interactions from a natural bond orbital, donor-acceptor viewpoint. Chem Rev 88:899–926
69. Reed AE, Weinstock RB, Weinhold F (1985) Natural population analysis. J Chem Phys 83:735–746
70. Keith TA (2014) AIMAll (Version 14.06.21). TK Gristmill Software, Overland Park
71. Kozlowski D, Trouillas P, Calliste C, Marsal P, Lazzaroni R, Duroux J-L (2007) Density functional theory study of the conformational, electronic, and antioxidant properties of natural chalcones. J Phys Chem A 111:1138–1145
72. Trouillas P, Marsal P, Svobodová A, Vostálová J, Gažák R, Hrbáč J, Sedmera P, Křen V, Lazzaroni R, Duroux J-L, Walterová D (2008) Mechanism of the antioxidant action of silybin and 2,3-dehydrosilybin flavonolignans: a joint experimental and theoretical study. J Phys Chem A 112:1054–1063
73. Foti MC, Barclay LRC, Ingold KU (2002) The role of hydrogen bonding on the h-atom-donating abilities of catechols and naphthalene diols and on a previously overlooked aspect of their infrared spectra. J Am Chem Soc 124:12881–12888
74. Foti MC (2007) Antioxidant properties of phenols. J Pharm Pharmacol 59:1673–1685
75. Osorio E, Pérez EG, Areche C, Ruiz LM, Cassels BK, Flórez E, Tiznado W (2013) Why is quercetin a better antioxidant than taxifolin? Theoretical study of mechanisms involving activated forms. J Mol Model 19:2165–2172
76. Litwinienko G, Ingold KU (2003) Abnormal solvent effects on hydrogen atom abstractions. 1. The reactions of phenols with 2,2-diphenyl-1-picrylhydrazyl (dpph*) in alcohols. J Org Chem 68:3433–3438
77. Litwinienko G, Ingold KU (2004) Abnormal solvent effects on hydrogen atom abstraction. 2. Resolution of the curcumin antioxidant controversy. The role of sequential proton loss electron transfer. J Org Chem 69:5888–5896
78. Litwinienko G, Ingold KU (2005) Abnormal solvent effects on hydrogen atom abstraction. 3. Novel kinetics in sequential proton loss electron transfer chemistry. J Org Chem 70:8982–8990
79. Zhang H-Y, Ji H-F (2006) How vitamin E scavenges DPPH radicals in polar protic media. New J Chem 30:503–504
80. Platts JA, Howard ST, Bracke BRF (1996) Directionality of hydrogen bonds to sulfur and oxygen. J Am Chem Soc 118:2726–2733
81. Perez-Lustres JL, Bräuer M, Mosquera M, Clark T (2001) Ground-state tautomerism and rotational isomerization in 4,5-dimethyl-2-(2-hydroxyphenyl)imidazole in the gas phase and in polar solvents: a theoretical study of the aromaticity, intramolecular hydrogen-bond strength and differential solute–solvent interactions. Phys Chem Chem Phys 3:3569–3579
82. Gogoi U, Guha AK, Phukan AK (2011) Nature of intramolecular metal–metal interactions in supported group 4–group 9 and group 6–group 9 heterobimetallic complexes: a combined density functional theory and topological Study. Organometallics 30:5991–6002
83. Bader RFW, Matta CF (2001) Bonding in Titanium. Inorg Chem 40:5603–5611
84. Gervasio G, Bianchi R, Marabello D (2004) About the topological classification of the metal–metal bond. Chem Phys Lett 387:481–484
85. Kabanda MM, Tran VT, Tran TQ, Ebenso EE (2014) Computational study of pyrazinamide: tautomerism, acid-base properties, micro-solvation effects and acid hydrolysis mechanism. Comput Theor Chem 1046:30–41
86. Tsiepe TJ, Kabanda MM, Serobatse KRN (2015) Antioxidant properties of kanakugiol revealed through the hydrogen atom transfer, electron transfer and M^{2+} (M^{2+} = Cu(II) or Co(II) ion) coordination ability mechanisms. A DFT study *in vacuo* and in solution. Food Biophys. doi:10.1007/s11483-015-9397-0
87. Feng L, Bai F-Q, Wu Y, Zhang H-X (2011) Dihydrogen bond in $C_2H_4 - n$ Cl $n \cdots$NaH ($n = 0, 1, 2, 3$) complexes: ab initio, AIM and NBO studies. Mol Phys 109:645–653
88. Varadwaj PR, Marques HM (2010) The physical chemistry of coordinated aqua-, ammine-, and mixed-ligand Co^{2+} complexes: DFT studies on the structure, energetics, and topological properties of the electron density. Phys Chem Chem Phys 12:2126–2136
89. Espinosa E, Alkorta I, Elguero J, Molins E (2002) From weak to strong interactions: a comprehensive analysis of the topological and energetic properties of the electron density distribution involving X-H···F-Y systems. J Chem Phys 117:5529–5542